Multiphoton quantum Rabi oscillations in ultrastrong cavity QED

Luigi Garziano,[1,2] Roberto Stassi,[1,2] Vincenzo Macrì,[1] Anton Frisk Kockum,[2] Salvatore Savasta,[1,2] and Franco Nori[2,3]

[1]*Dipartimento di Fisica e di Scienze della Terra, Università di Messina, I-98166 Messina, Italy*

[2]*CEMS, RIKEN, Saitama 351-0198, Japan*

[3]*Department of Physics, University of Michigan, Ann Arbor, Michigan 48109-1040, USA*

When an atom is strongly coupled to a cavity, the two systems can exchange a *single* photon through a coherent Rabi oscillation. This process enables precise quantum-state engineering and manipulation of atoms and photons in a cavity, which play a central role in quantum information and measurement. Recently, a new regime of cavity QED was reached experimentally where the strength of the interaction between light and artificial atoms (qubits) becomes comparable to the atomic transition frequency or the resonance frequency of the cavity mode. Here we show that this regime can strongly modify the concept of vacuum Rabi oscillations, enabling multiphoton exchanges between the qubit and the resonator. We find that experimental state-of-the-art circuit-QED systems can undergo *two-* and *three*-photon vacuum Rabi oscillations. These anomalous Rabi oscillations can be exploited for the realization of efficient Fock-state sources of light and complex entangled states of qubits.

I. INTRODUCTION

Light-matter interaction in the strong-coupling regime is a coherent reversible process in which a photon is absorbed and reemitted by an electronic transition at a rate equal to the coupling energy divided by the Planck constant [1,2]. Reaching the light-matter strong-coupling regime has been a major focus of research in atomic physics and quantum optics for several decades and has driven the field of cavity quantum electrodynamics (QED) [3,4]. The strong-coupling regime has been observed, in both the time and frequency domains, in a variety of systems [5], when an electronic transition is resonantly coupled to a cavity (optical resonator) and the coupling rate exceeds the rates of relaxation and decoherence of both the electronic transition and the field. Cavity QED effects with individual qubits have been intensively studied in solid state systems by replacing natural atoms with artificial atoms, such as quantum dots [6,7] and Josephson circuits [8–11]. The strong-coupling regime, when reached with a single qubit, enables a high degree of manipulation and control of quantum systems [12]. For example, by exploiting the strong-coupling regime of cavity QED, the preparation and measurement of arbitrary quantum states in a completely controlled and deterministic manner have been achieved [13,14] and Schrödinger's cat states of radiation have been prepared and reconstructed [15,16]. Basic steps in quantum information processing, including the deterministic entanglement of atoms and the realization of quantum gates using atoms and photons as quantum bits, have also been demonstrated [2,17,18].

Recently, a new regime of cavity QED, where the coupling rate becomes an appreciable fraction of the unperturbed frequency of the bare systems, has been experimentally reached in a variety of solid state systems [19–27]. In this so-called ultrastrong-coupling (USC) regime, the routinely invoked rotating-wave approximation (RWA) is no longer applicable and the antiresonant terms in the interaction Hamiltonian significantly change the standard cavity QED scenarios (see, e.g., Refs. [28–36]). Although in principle counterrotating terms exist in any real light-matter interaction Hamiltonian, their effects become prominent only in the USC limit [37].

Usually, light-matter USC is reached by coupling the resonator with a large number of molecules or more generally electronic transitions. Ultrastrong coupling with a single qubit has been achieved only by using superconducting circuits based on Josephson junctions, which exhibit macroscopic quantum coherence and giant dipole moments as artificial atoms [20,21,38].

One interesting feature of the USC regime is that the number of excitations in the cavity-emitter system is no longer conserved, even in the absence of drives and dissipation. Measurements on a superconducting circuit QED system in the USC regime have shown clear evidence of this feature [21]. Specifically, by tuning the qubit transition frequency (by adjusting the external flux bias threading the qubit) and measuring the cavity transmission, an anticrossing arising from the coupling between states with a different number of excitations has been observed. In particular, the measurements evidence the resonant coupling of the states $|\phi_1\rangle = |g,0,0,1\rangle$ and $|\phi_2\rangle = |e,1,0,0\rangle$, where the kets indicate the states of the qubit and of the first three resonator modes. This level anticrossing occurs when $\omega_q + \omega_1^r \approx \omega_3^r$, where ω_q is the transition frequency of the artificial atom and the ω_m^r are the resonance frequencies of the cavity modes. The dominant contributions to the resulting eigenstates $|\psi_\pm\rangle$ are approximate symmetric and antisymmetric superpositions of the degenerate states $|\phi_1\rangle$ and $|\phi_2\rangle$. The coupling between these two states, determining the anticrossing, originates from counterrotating terms in the interaction Hamiltonian that do not conserve the number of excitations. Indeed, the resulting effect of the action of these counterrotating terms on, e.g., the $|\phi_2\rangle$ state is the annihilation of two excitations, one in the $m = 1$ mode and one in the qubit, and the simultaneous creation of a single excitation in the $m = 3$ mode. Such a process can result only from counterrotating terms, but it would not be possible within the RWA.

Very recently it was shown [39] that, when the frequency of the cavity field is near one-third of the atomic transition frequency, there exists a resonant three-photon coupling via intermediate states connected by counterrotating processes. The resonant quantum Rabi oscillations, occurring when

the atom and the cavity mode can exchange one excitation quantum in a reversible way, play a key role in the manipulation of atomic and field states for quantum information processing [12]. Here we show that a system consisting of a single qubit coupled ultrastrongly to a resonator can exhibit anomalous vacuum Rabi oscillations where *two* or *three* photons are jointly emitted by the qubit into the resonator and reabsorbed by the qubit in a reversible and coherent process. We focus on the case of a flux qubit coupled to a coplanar-waveguide resonator, a system where the USC regime with a single artificial atom has been demonstrated [21]. We find that this effect can be observed at coupling rates of the same order as those already reached in these systems [21,38].

II. DISSIPATION AND PHOTODETECTION IN THE USC REGIME

In order to demonstrate multiphoton quantum Rabi oscillations in USC cavity QED, we calculate the time evolution of the mean output photon fluxes and higher-order normally ordered photon correlations. It has been shown that, in the USC regime, the usual normally ordered correlation functions fail to describe the output photon emission rate and photon statistics. Clear evidence of this is that the standard input-output relations predict, even for a vacuum input and the system in the ground state, a finite output photon flux proportional to the average number of cavity photons [32,40,41], i.e., $\langle \hat{A}_{out}^-(t)\hat{A}_{out}^+(t)\rangle \propto \langle \hat{a}^\dagger(t)\hat{a}(t)\rangle$, where $\hat{A}_{out}^+(t)$ and $\hat{A}_{out}^-(t)$ are the positive- and negative-frequency components of the output field operator and $\hat{a}$ and $\hat{a}^\dagger$ are the destruction and creation operators for cavity photons. A solution to this problem was proposed in Ref. [32]. Considering, for the sake of simplicity, a single-mode resonator, it is possible to derive the correct output photon emission rate and correlation functions by expressing the cavity electric-field operator $\hat{X} = \hat{a} + \hat{a}^\dagger$ in the atom-cavity dressed basis. Once the cavity electric-field operator has been expressed in the dressed basis, it has to be decomposed into its positive- and negative-frequency components $\hat{X}^+$ and $\hat{X}^-$ [32]. Expanding the $\hat{X}$ operator in terms of the energy eigenstates $|j\rangle$ (with $\hbar\omega_j$ the corresponding eigenvalues) of the system Hamiltonian $\hat{H}$, one finds the relations

$$\hat{X}^+ = \sum_{j,k>j} X_{jk}|j\rangle\langle k|, \quad \hat{X}^- = (\hat{X}^+)^\dagger, \tag{1}$$

where $X_{jk} \equiv \langle j|(\hat{a}^\dagger + \hat{a})|k\rangle$ and the states are labeled such that $\omega_k > \omega_j$ for $k > j$. The resulting positive frequency output operator can be expressed as

$$\hat{A}_{out}^+(t) = \hat{A}_{in}^+(t) - \sqrt{\kappa}C_0\hat{X}^+, \tag{2}$$

where κ is the loss rate of the resonator due to the coupling to the external in-out modes and C_0 is a constant proportional to the zero-point fluctuation amplitude of the resonator [42]. Two aspects of these results are noteworthy. First of all, we note that in the USC regime, one correctly obtains $\hat{X}^+|0\rangle = 0$ for the system in its ground state $|0\rangle$ in contrast to $\hat{a}|0\rangle \neq 0$. Moreover, we note that the positive-frequency component of $\hat{X}$ is not simply proportional to the photon annihilation operator $\hat{a}$. As a consequence, for arbitrary degrees of light-matter interaction, the output photon flux emitted by a resonator

can be expressed as $\Phi_{out} = \kappa\langle \hat{X}^-\hat{X}^+\rangle$. Similarly, the output delayed coincidence rate is proportional to the two-photon correlation function $\langle \hat{X}^-(t)\hat{X}^-(t+\tau)\hat{X}^+(t+\tau)\hat{X}^+(t)\rangle$. In quantum optics, it is well known that the signal directly emitted from the qubit is proportional to $\langle \hat{\sigma}_+\hat{\sigma}_-\rangle$. In circuit QED systems, this emission can be detected by coupling the qubit to an additional microwave antenna [14]. Indeed, in the USC regime the qubit emission rate becomes proportional to the qubit mean excitation number $\langle \hat{C}^-\hat{C}^+\rangle$, where $\hat{C}^\pm$ are the qubit positive- and negative-frequency operators, defined as $\hat{C}^+ = \sum_{j,k>j} C_{jk}|j\rangle\langle k|$ and $\hat{C}^- = (\hat{C}^+)^\dagger$, with $C_{jk} \equiv \langle j|(\hat{\sigma}_- + \hat{\sigma}_+)|k\rangle$.

In order to properly describe the system dynamics, including dissipation and decoherence effects, the coupling to the environment needs to be considered. We adopt the master-equation approach. However, in the USC regime the description offered by the standard quantum-optical master equation breaks down [43]. Following Refs. [41,44], we express the system-bath interaction Hamiltonian in the basis formed by the energy eigenstates of $\hat{H}$. We consider $T = 0$ temperature reservoirs (the generalization to $T \neq 0$ reservoirs is straightforward). By applying the standard Markov approximation and tracing out the reservoir degrees of freedom, we arrive at the master equation for the density-matrix operator $\hat{\rho}(t)$,

$$\dot{\hat{\rho}} = \frac{i}{\hbar}[\hat{\rho}(t),\hat{H}] + \mathcal{L}_{damp}\hat{\rho}(t) + \mathcal{L}_\phi\hat{\rho}(t), \tag{3}$$

where $\mathcal{L}_{damp}\hat{\rho}(t) = \sum_{j,k>j}(\Gamma_\kappa^{jk} + \Gamma_\gamma^{jk})\mathcal{D}[|j\rangle\langle k|]\hat{\rho}(t)$, with $\mathcal{D}[\hat{O}]\hat{\rho} = \frac{1}{2}(2\hat{O}\hat{\rho}\hat{O}^\dagger - \hat{\rho}\hat{O}^\dagger\hat{O} - \hat{O}^\dagger\hat{O}\hat{\rho})$, describes dissipation effects arising from the resonator and qubit reservoirs. These cause transitions between eigenstates at rates

$$\Gamma_\kappa^{jk} = \kappa|\langle j|\hat{X}|k\rangle|^2, \tag{4}$$

$$\Gamma_\gamma^{jk} = \gamma|\langle j|\hat{\sigma}_x|k\rangle|^2, \tag{5}$$

where κ and γ are decay rates, here assumed to be spectrally constant, induced by the resonator and qubit reservoirs. Pure dephasing effects affecting the qubit are described in Eq. (3) by the last term $\mathcal{L}_\phi\hat{\rho}(t) = \mathcal{D}[\sum_j \Phi_j|j\rangle\langle j|]\hat{\rho}(t)$, where $\Phi_j = \sqrt{\gamma_\phi/2}\langle j|\hat{\sigma}_z|j\rangle$, and γ_ϕ is the pure dephasing rate. Note that only the most relevant diagonal contributions have been included.

III. RESULTS

Here we study a flux qubit coupled to a coplanar resonator in the USC regime. For suitable junctions, the qubit potential landscape is a double-well potential, where the two minima correspond to states with clockwise and counterclockwise persistent currents $\pm I_p$ [10,11]. When the flux offset $\delta\Phi_x \equiv \Phi_{ext} - \Phi_0/2 = 0$, where Φ_{ext} is the external flux threading the qubit and Φ_0 is the flux quantum, the two lowest-energy states are separated by an energy gap Δ. In the qubit eigenbasis, the qubit Hamiltonian reads $\hat{H}_q = \hbar\omega_q\hat{\sigma}_z/2$, where $\hbar\omega_q = \sqrt{\Delta^2 + (2I_p\delta\Phi_x)^2}$ is the qubit transition frequency, which can be adjusted by an external flux bias. We note that the two-level approximation is well justified because of the large anharmonicity of this superconducting artificial atom.

The resonator modes are described as harmonic oscillators $\hat{H}_m = \hbar \omega_m^r \hat{a}_m^\dagger \hat{a}_m$, where ω_m^r is the resonance frequency, m is the resonator-mode index, and $\hat{a}_m^\dagger$ ($\hat{a}_m$) is the bosonic creation (annihilation) operator for the mth resonator mode. We will consider $\lambda/2$ and $\lambda/4$ resonators. Then the quantum circuit can be described by the extended Rabi Hamiltonian

$$\hat{H} = \hat{H}_q + \sum_m [\hat{H}_m + \hbar g_m \hat{X}_m (\cos\theta \hat{\sigma}_x + \sin\theta \hat{\sigma}_z)]. \quad (6)$$

Here $\hat{X}_m = \hat{a}_m + \hat{a}_m^\dagger$, $\hat{\sigma}_{x,z}$ denote Pauli operators, g_m is the coupling rate of the qubit to the mth cavity mode, and the flux dependence is encoded in $\cos\theta = \Delta/\omega_q$. The operator $\hat{\sigma}_x$ is conveniently expressed as the sum of the qubit raising $\hat{\sigma}_+$ and lowering $\hat{\sigma}_-$ operators, which in the Heisenberg picture and for $g_m = 0$ oscillate as $\exp(i\omega_q t)$ (negative frequency) and $\exp(-i\omega_q t)$ (positive frequency), respectively. Thus, in contrast to the Jaynes-Cummings (JC) model [45], the Hamiltonian in Eq. (6) explicitly contains counterrotating terms of the form $\hat{\sigma}_+ \hat{a}_m^\dagger$, $\hat{\sigma}_- \hat{a}_m$, $\hat{\sigma}_z \hat{a}_m^\dagger$, and $\hat{\sigma}_z \hat{a}_m$. Considering only one resonator mode and a flux offset $\delta\Phi_x = 0$, the Hamiltonian in Eq. (6) reduces to the standard Rabi Hamiltonian.

A. Two-photon quantum Rabi oscillations

We first consider the case of a flux qubit coupled to a $\lambda/2$ superconducting transmission-line resonator with resonance frequencies $\omega_m^r = m\pi c/L$, where L is the resonator length. We use the qubit parameters $\Delta/h = 2.25$ GHz and $2I_p = 630$ nA, as in Ref. [21]. We are interested in the situation where the qubit transition energy is approximately twice that of the fundamental resonator mode: $\omega_q \approx 2\omega_1^r$. We consider the qubit to be positioned at the center of the resonator so that it does not interact with the resonator mode $m = 2$ [see Fig. 1(a)]. The other resonator modes are much higher in energy, detuned with respect to the qubit transition frequency by an amount significantly larger than the coupling rate $\omega_m^r - \omega_q \approx (m - 2)\omega_1^r$, providing only moderate energy shifts for the coupling rates $g_m/\omega_m^r \lesssim 0.2$ considered here. We will thus only take into account the interaction of the qubit with the fundamental resonator mode. We diagonalize numerically the Hamiltonian from Eq. (6) and indicate the resulting energy eigenvalues and eigenstates as $\hbar\omega_i$ and $|i\rangle$ with $i = 0, 1, \ldots,$ choosing the labeling of the states such that $\omega_k > \omega_j$ for $k > j$.

Figure 1(b) shows the frequency differences $\omega_{i,0} = \omega_i - \omega_0$ for the lowest-energy states as a function of the qubit transition frequency, which can be tuned by changing the external flux bias $\delta\Phi_x$. The red dashed curves correspond to calculations obtained neglecting all the counterrotating terms (the JC model). We observe a spectrum with two large-splitting anticrossings around $\omega_q \approx \omega_1^r$, which appear for both the dashed and the solid curves. In the JC picture, they correspond to the resonant coupling between states with the same number of excitations. The lowest-energy avoided crossing results from the coherent coupling of the states $|e,0\rangle$ and $|g,1\rangle$, where g (e) indicates the ground (excited) state of the qubit and the second entry in the kets represents the photon number. When the splitting reaches its minimum, the resulting system
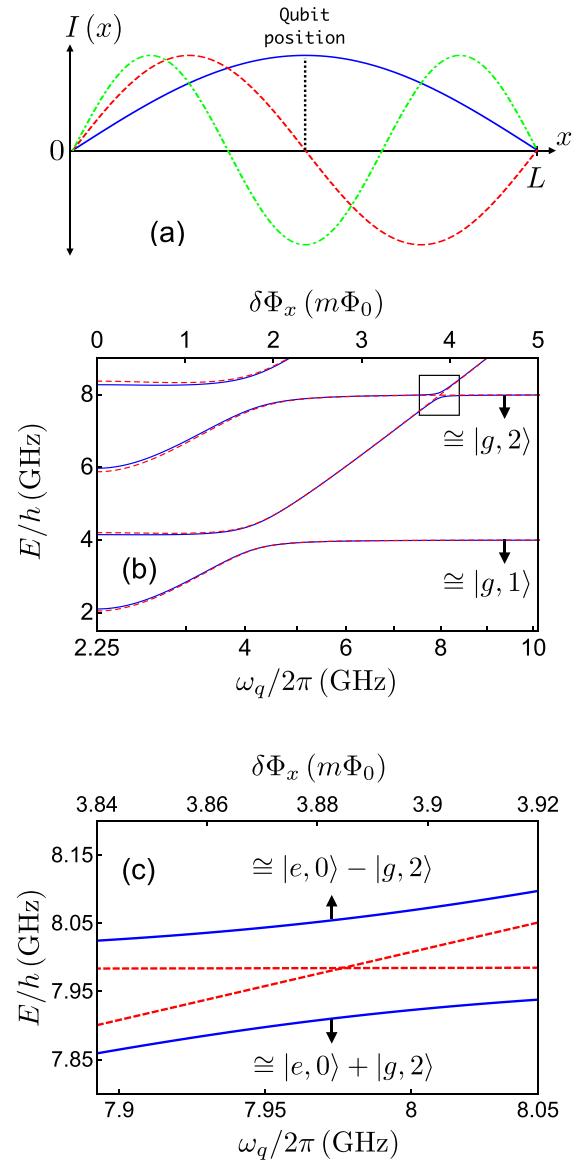

FIG. 1. (Color online) (a) Sketch of the distribution of the first three resonator modes $m = 1,2,3$ of a transmission-line $\lambda/2$ resonator. The resonance frequency of the first mode (blue solid curve) is set to $\omega_1^r/2\pi = 4$ GHz. The qubit is positioned at the center of the resonator so that it does not interact with the mode $m = 2$ (red dashed curve) and is off-resonance with the mode $m = 3$ (green dot-dashed curve) mode. The bare resonance frequencies of the second and third modes are $\omega_2^r = 2\omega_1^r$ and $\omega_3^r = 3\omega_1^r$, respectively. The qubit parameters are $\Delta/h = 2.25$ GHz and $2I_p = 630$ nA. (b) Frequency differences $\omega_{i,0} = \omega_i - \omega_0$ for the lowest-energy dressed states as a function of the qubit transition frequency ω_q (which can be tuned by changing the external flux bias $\delta\Phi_x$) for the JC model (red dashed curves) and the extended Rabi Hamiltonian (blue solid curves). We consider a normalized coupling rate $g_1/\omega_1^r = 0.15$ between the qubit and the resonator. In both cases the ground state level is not displayed. (c) Avoided level crossing (blue solid curves) resulting from the coupling between the states $|e,0\rangle$ and $|g,2\rangle$ due to the presence of counterrotating terms in the system Hamiltonian. The energy splitting reaches its minimum at $\omega_q/2\pi \approx 7.97$ GHz $\approx 2(\omega_1^r/2\pi)$. The anticrossing is not present in the JC model (red dashed lines), since it arises from the coherent coupling between states with a different number of excitations.

eigenstates are

$$\frac{1}{\sqrt{2}}(|e,0\rangle \pm |g,1\rangle).\tag{7}$$

The higher-energy large avoided crossing in the plot corresponds to the second rung of the JC ladder, arising from the coupling of $|e,1\rangle$ and $|g,2\rangle$. Only small quantitative deviations between the eigenenergies in the JC and in the extended Rabi model can be observed.

When the counterrotating terms are taken into account, the states $|i\rangle$ are no longer eigenstates of the total number of the excitation operator $\hat{N}_{\rm exc} = \hat{a}^{\dagger}a + \hat{\sigma}_{+}\hat{\sigma}_{-}$. For example, the system ground state can be expressed as a superposition $|0\rangle = \sum_n c_{gn}^0 |g,n\rangle + c_{en}^0 |e,n\rangle$ of bare states also involving nonzero excitations. Of course, when the normalized coupling $g_1/\omega_1^{\rm r} \ll 1$, only the coefficient c_{g0}^0 is significantly different from zero. Moreover, for $\theta = 0$ parity is conserved [46,47] and only states with an even number of excitations contribute to $|0\rangle$. The nonconservation of the total excitation number also affects the excited dressed states $|j\rangle = \sum_n c_{gn}^j |g,n\rangle + c_{en}^j |e,n\rangle$. As a consequence, the dressed states $|1\rangle$ and $|2\rangle$ at the minimum splitting do not correspond to the simple JC picture of Eq. (7).

The solid line levels in Fig. 1(b) also display a smaller-amplitude avoided crossing when $\omega_{\rm q} \approx 2\omega_1^{\rm r}$. Observing that just outside this avoided-crossing region one level remains flat as a function of the flux offset $\delta\Phi_x$ with energy $\omega \approx 2\omega_1^{\rm r}$ while the other shows a linear behavior with $\omega_{\rm q}$, the splitting originates from the hybridization of the states $|e,0\rangle$ and $|g,2\rangle$. This avoided crossing behavior is better shown in Fig. 1(c) and the resulting states are well approximated by the states $\frac{1}{\sqrt{2}}(|e,0\rangle \pm |g,2\rangle)$. This splitting is not present in the RWA, where the coherent coupling between states with a different number of excitations is not allowed, nor does it occur with the standard Rabi Hamiltonian ($\theta = 0$).

Following the procedure described in Ref. [39], such a two-photon coupling between the bare states $|e,0\rangle$ and $|g,2\rangle$ can be analytically described by an effective Hamiltonian (see the Appendix). As displayed in Fig. 2, the coupling between $|e,0\rangle$ and $|g,2\rangle$ can only occur via the intermediate states $|g,1\rangle$ and $|e,1\rangle$. Indeed, if the system is initially prepared in the state $|e,0\rangle$, two different processes can occur: Either (i) the counterrotating term $\hat{a}_1^{\dagger}\hat{\sigma}_z$ enables a virtual transition
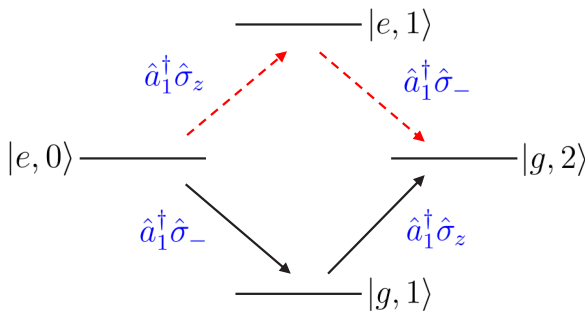

FIG. 2. (Color online) Coupling between the bare states $|e,0\rangle$ and $|g,2\rangle$ via the intermediate states $|g,1\rangle$ and $|e,1\rangle$. The red dashed arrows and the solid black arrows indicate, respectively, the two different processes describing the two-photon resonant coupling between $|e,0\rangle$ and $|g,2\rangle$.

$|e,0\rangle \to |e,1\rangle$ and then the term $\hat{a}_1^{\dagger}\hat{\sigma}_-$ leads to the final transition to the state $|g,2\rangle$ or (ii) the term $\hat{a}_1^{\dagger}\hat{\sigma}_-$ enables the transition $|e,0\rangle \to |g,1\rangle$, which is followed by the virtual transition $|g,1\rangle \to |g,2\rangle$ induced by the term $\hat{a}_1^{\dagger}\hat{\sigma}_z$.

In order to obtain an analytical description of the effective coupling, we first reduce the extended Rabi Hamiltonian to the truncated Hilbert space composed of the bare states $|e,0\rangle$, $|g,1\rangle$, $|e,1\rangle$, and $|g,2\rangle$. The matrix form of the reduced Hamiltonian becomes

$$\frac{\hat{H}_{\rm r}}{\hbar} = \begin{pmatrix} \frac{\omega_{\rm q}}{2} & g_1\cos\theta & g_1\sin\theta & 0 \\ g_1\cos\theta & \omega_1^{\rm r} - \frac{\omega_{\rm q}}{2} & 0 & -\sqrt{2}g_1\sin\theta \\ g_1\sin\theta & 0 & \omega_1^{\rm r} + \frac{\omega_{\rm q}}{2} & \sqrt{2}g_1\cos\theta \\ 0 & -\sqrt{2}g_1\sin\theta & \sqrt{2}g_1\cos\theta & 2\omega_1^{\rm r} - \frac{\omega_{\rm q}}{2} \end{pmatrix},\tag{8}$$

where the order of columns and rows is $|e,0\rangle$, $|g,1\rangle$, $|e,1\rangle$, and $|g,2\rangle$. Near the two-photon resonance when $\omega_{\rm q} \approx 2\omega_1^{\rm r}$, the intermediate states $|g,1\rangle$ and $|e,1\rangle$ can be adiabatically eliminated (see the Appendix), leading to the effective Hamiltonian

$$\hat{H}_{\rm eff} = \left(\frac{\omega_{\rm q}}{2} + \frac{2g_1^2}{\omega_{\rm q}}\cos(2\theta)\right)|e,0\rangle\langle e,0|$$

$$+ \left(2\omega_1^{\rm r} - \frac{\omega_{\rm q}}{2} - \frac{4g_1^2}{\omega_{\rm q}}\cos(2\theta)\right)|g,2\rangle\langle g,2|$$

$$- \Omega_{\rm eff}^{(2{\rm ph})}(|e,0\rangle\langle g,2| + |g,2\rangle\langle e,0|),\tag{9}$$

which describes the effective two-photon coupling between $|e,0\rangle$ and $|g,2\rangle$, with an effective two-photon Rabi frequency

$$\Omega_{\rm eff}^{(2{\rm ph})} \equiv \frac{2\sqrt{2}g_1^2\sin(2\theta)}{\omega_{\rm q}}.\tag{10}$$

A key theoretical issue of the USC regime is the distinction between bare (unobservable) excitations and physical particles that can be detected. For example, when the counterrotating terms are relevant, the mean photon number in the system ground state is different from zero, $\langle 0|\hat{a}^{\dagger}\hat{a}|0\rangle \neq 0$. However, these photons are actually virtual since they do not correspond to real particles that can be detected in a photon-counting experiment. According to this analysis, the presence of an n-photon contribution in a specific eigenstate of the system does not imply that the system can emit n photons when prepared in this state. In order to fully understand and characterize this avoided crossing not present in the RWA, a more quantitative analysis is required. In the following, we therefore calculate the output signals and correlations that can be measured in a photodetection experiment.

In order to probe the anomalous avoided crossing shown in Figs. 1(b) and 1(c), we consider the case where the qubit is directly excited via a microwave antenna by an optical Gaussian pulse. The corresponding driving Hamiltonian is

$$\hat{H}_{\rm d} = \mathcal{E}(t)\cos(\omega t)\hat{\sigma}_x,\tag{11}$$

where $\mathcal{E}(t) = A\exp\left[-(t - t_0)^2/2\tau^2\right]/\tau\sqrt{2\pi}$. Here A and τ are the amplitude and the standard deviation of the Gaussian pulse, respectively. We consider the zero-detuning case by choosing the flux offset $\delta\Phi_x$ corresponding to the qubit frequency $\omega_{\rm q}/2\pi \simeq 7.97$ GHz, where the splitting in Fig. 1(b)
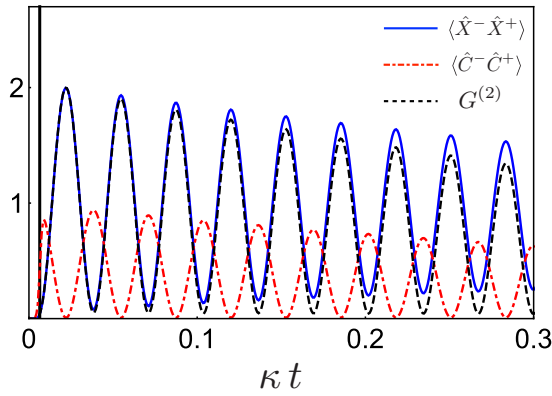
FIG. 3. (Color online) Time evolution of the cavity mean photon number $\langle \hat{X}^- \hat{X}^+ \rangle$ (blue solid curve), the qubit mean excitation number $\langle \hat{C}^- \hat{C}^+ \rangle$ (red dot-dashed curve), and the zero-delay two-photon correlation function $G^{(2)}(t)$ (dashed black curve) after the arrival of a π-like Gaussian pulse initially exciting the qubit (the black vertical line on the far left shows the wave-packet peak arrival time). The amplitude and the central frequency of the pulse are $A/\omega_1^r = 8.7 \times 10^{-2}$ and $\omega = (\omega_{3,0} + \omega_{2,0})/2$, respectively. After the arrival of the pulse, the system undergoes vacuum Rabi oscillations showing the reversible excitation exchange of two photons between the qubit and the resonator. Initially, $\langle \hat{X}^- \hat{X}^+ \rangle$ and $G^{(2)}(t)$ almost coincide. This perfect two-photon correlation is a signature that photons are actually emitted in pairs. The resonator and qubit damping rates are $\kappa/\omega_1^r = 1.8 \times 10^{-4}$ and $\gamma/\omega_1^r = 1.8 \times 10^{-4}$, respectively.

is at its minimum. The central frequency of the pulse has been chosen to be in the middle of the two split transition energies $\omega = (\omega_{3,0} + \omega_{2,0})/2$.

The cavity output photon flux and the photon flux emitted by the qubit directly coupled to a microwave antenna are proportional to $\langle \hat{X}^- \hat{X}^+ \rangle$ and $\langle \hat{C}^- \hat{C}^+ \rangle$, respectively. Figure 3 displays the dynamics of these two quantities and of the zero-delay two-photon correlation function $G^{(2)}(t) = \langle \hat{X}^-(t)\hat{X}^-(t)\hat{X}^+(t)\hat{X}^+(t) \rangle$ (dashed black curve) after the arrival of a π-like pulse initially exciting the qubit described by the Hamiltonian (11). Calculations in Fig. 3 have been carried out in the absence of pure dephasing ($\gamma_\phi = 0$). Results for $\gamma_\phi \neq 0$ are shown in Fig. 4. Vacuum Rabi oscillations showing the reversible excitation exchange between the qubit and the resonator are clearly visible in Fig. 3. The pulse time width is not much narrower than the Rabi period, so the qubit excitation is partially transferred to the cavity during the pulse arrival. Therefore, the first peak of the qubit mean excitation number in Fig. 3 is slightly lower than the second one. We observe that the mean intracavity physical photon number at its first maximum is very close to 2. This is an initial hint that when the qubit is in the ground state the resonator mode acquires two photons. However, the output measured signals are proportional and not equal to $\langle \hat{X}^- \hat{X}^+ \rangle$, so from this kind of measurement it is not possible to certify that the qubit and the resonator are actually exchanging two quanta. We also observe that at early times $\langle \hat{X}^- \hat{X}^+ \rangle$ and $G^{(2)}(t)$ almost coincide. This is a signature of perfect two-photon correlation: The probability of the system to emit one photon is equal to the probability to emit a photon pair. During the system evolution, higher values of the local minima of $\langle \hat{X}^- \hat{X}^+ \rangle$ are observed due to the decay from the
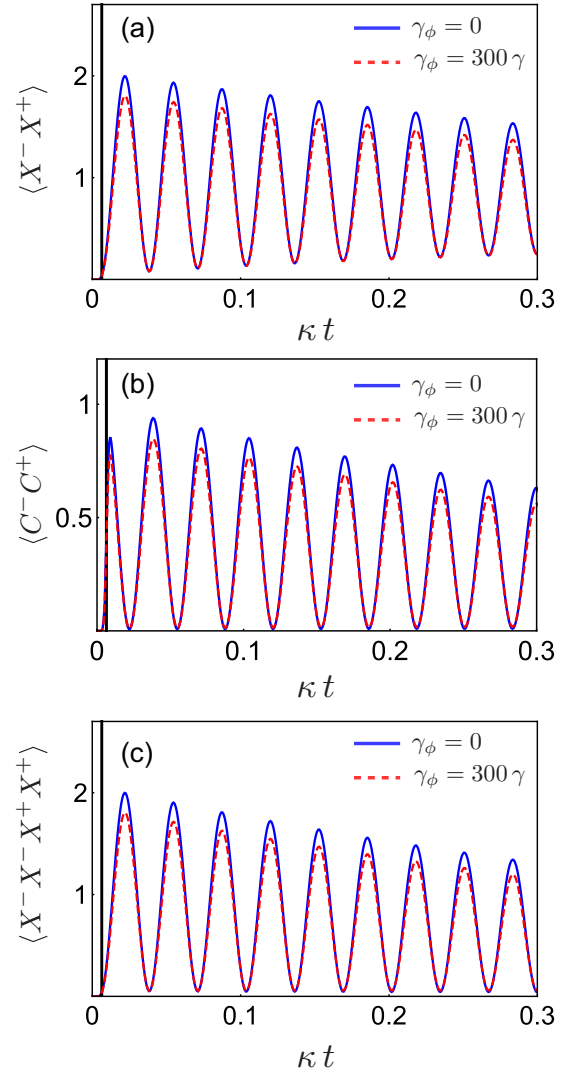

FIG. 4. (Color online) Effects of strong pure dephasing (dashed curves) on the dynamics of (a) the mean photon number $\langle \hat{X}^- \hat{X}^+ \rangle$, (b) the effective qubit population $\langle \hat{C}^- \hat{C}^+ \rangle$, and (c) the two-photon correlation function $\langle \hat{X}^- \hat{X}^- \hat{X}^+ \hat{X}^+ \rangle$. Calculations have been performed with the same parameters as in Fig. 3 with the addition of a pure dephasing rate $\gamma_\phi = 300\gamma$. Solid curves display numerical results obtained in the absence of pure dephasing, $\gamma_\phi = 0$. It can be observed that the physics of multiphoton vacuum Rabi oscillations is not significantly altered by the effects of pure dephasing.

two-photon state to the one-photon state (out of resonance with respect to the qubit) caused by the photon escape from the resonator. However, the two-photon correlation function $\langle \hat{X}^-(t)\hat{X}^-(t)\hat{X}^+(t)\hat{X}^+(t) \rangle$ goes almost to zero every time the qubit is maximally excited. This different behavior indicates that the qubit does not absorb single photons but only photon pairs. The period of a complete population oscillation is $2\pi/\Omega_{\mathrm{eff}}^{(2\mathrm{ph})}$, where $2\Omega_{\mathrm{eff}}^{(2\mathrm{ph})}$ is the minimum splitting in Fig. 1(c).

Ordinary quantum vacuum oscillations have already been demonstrated in circuit-QED systems (e.g., [10,48]). The dynamics observed in Fig. 3 can also be obtained by first preparing the qubit in its excited state by employing a π pulse.

Then the π pulse can be followed by a shift pulse that brings the qubit into resonance with the resonator for the desired duration in order to observe the coupled dynamics as in Ref. [48]. If the shift pulse has a duration $\delta t = 2\pi/\Omega_{\mathrm{eff}}^{(2\mathrm{ph})}$, the Fock state $n = 2$ is directly generated. After the switch-off of the shift pulse, the qubit is out of resonance with the resonator and the Fock state can escape from the cavity through an input-output port and be detected. Hence two-photon Rabi oscillations can be exploited for fast and efficient generation of two-photon states.

The influence of strong pure dephasing effects is shown in Fig. 4. Calculations have been performed with the same parameters used in Fig. 3 with the addition of a pure dephasing rate $\gamma_\phi = 300\gamma$. Figure 4 compares the dynamics of the mean photon number [Fig. 4(a)], the qubit effective population [Fig. 4(b)], and the two-photon correlation [Fig. 4(c)] in the absence (solid curves) and in the presence (dashed curves) of pure dephasing. The figure shows that strong pure dephasing does not significantly alter the physics of multiphoton vacuum Rabi oscillations and the main effect of dephasing is to make the excitation pulse less effective.

B. Three-photon quantum Rabi oscillations

Very recently, it was shown [39] that the strong coupling of a single qubit with three photons can be achieved in the USC regime when the frequency of the cavity field is near one-third of the atomic transition frequency. In this case, parity-symmetry breaking is not required and this effect can occur also at $\theta = 0$. Hence, it could be observed also in systems such as natural atoms or molecules displaying parity symmetry. One possible problem with this configuration is that the qubit can also interact resonantly with the one-photon state of the mode $m = 3$ of the resonator. In this case the qubit would interact with both one- and three-photon states. We show that the undesired one-photon resonant coupling of the qubit with a resonator mode can be avoided by considering a $\lambda/4$ resonator, whose resonance frequencies are $\omega_m^{\mathrm{r}} = (2m-1)\pi c/2L$, with $m = 1, 2, 3, \ldots$ [see Fig. 5(a)]. As shown in Fig. 5(a), the qubit is positioned so that it does not interact with the mode $m = 2$ with resonance frequency $\omega_2^{\mathrm{r}} = 3\omega_1^{\mathrm{r}}$. The qubit parameters are $\Delta/h = 4.25$ GHz and $2I_{\mathrm{p}} = 630$ nA. In the present case we are interested in the situation where the qubit transition energy is approximately three times that of the fundamental resonator mode $\omega_q \approx 3\omega_1^{\mathrm{r}}$. The mode $m = 3$ has resonance frequency $\omega_3^{\mathrm{r}} = 5\omega_1^{\mathrm{r}}$, which is much larger than ω_q. Hence, also in this case we can consider the interaction of the qubit with only the fundamental resonator mode.

Figure 5(b) displays the frequency differences $\omega_{i,0}$ for the lowest-energy states as a function of the qubit transition frequency. The red dashed curves corresponds to calculations obtained neglecting all the counterrotating terms (JC model). We observe a spectrum with two large-splitting anticrossings, which appear only in the solid curves plus a smaller avoided crossing magnified in Fig. 5(c). The lowest-energy splitting corresponds to a two-photon vacuum Rabi splitting. When it reaches its minimum (at $\omega_q \approx 2\omega_1^{\mathrm{r}}$), the corresponding hybridized states are analogous to those whose dynamics has been described in Fig. 3. They can be approximately
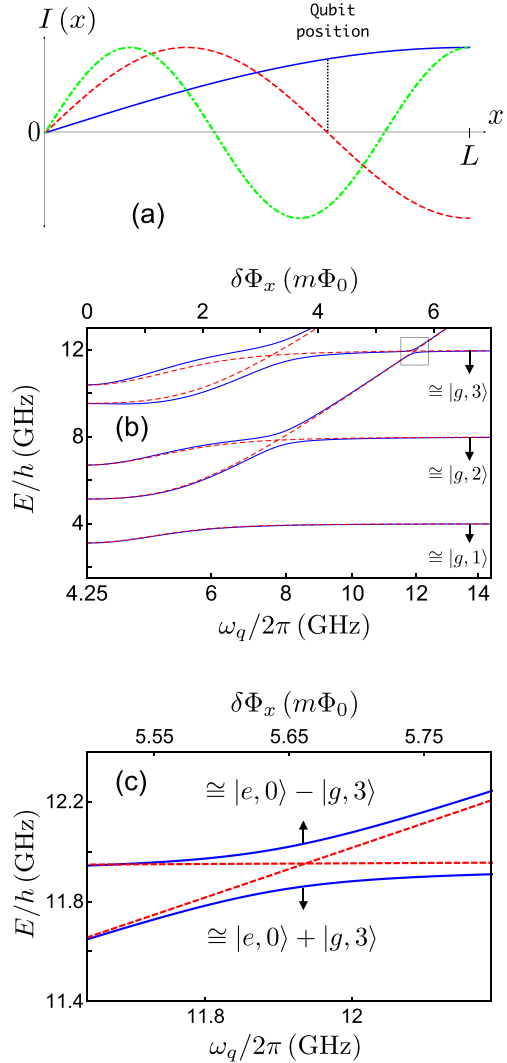

FIG. 5. (Color online) (a) Sketch of the distribution of the first three resonator modes $m = 1, 2, 3$ of a transmission-line $\lambda/4$ resonator. The resonance frequency of the first mode (blue solid curve) is $\omega_1^{\mathrm{r}} = 4$ GHz. The qubit is positioned so that it does not interact with the mode $m = 2$ (red dashed curve) with resonance frequency $\omega_2^{\mathrm{r}} = 3\omega_1^{\mathrm{r}}$. The mode $m = 3$ (green dot-dashed curve) has resonance frequency $\omega_3^{\mathrm{r}} = 5\omega_1^{\mathrm{r}}$, which is much larger than ω_q, so only the interaction of the qubit with the fundamental resonator mode must be considered. The qubit parameters are $\Delta/h = 4.25$ GHz and $2I_{\mathrm{p}} = 630$ nA. (b) Frequency differences $\omega_{i,0} = \omega_i - \omega_0$ for the lowest-energy dressed states as a function of the qubit transition frequency ω_q (which can be tuned by changing the external flux bias $\delta\Phi_x$) for the JC model (red dashed curves) and the extended Rabi Hamiltonian (blue solid curves) explicitly containing counterrotating terms. We consider a normalized coupling rate $g_1/\omega_1^{\mathrm{r}} = 0.25$ between the qubit and the resonator. The spectrum shows two large-splitting anticrossings, which appear only in the continuous curves, plus a smaller avoided crossing, which is magnified in (c). (c) Three-photon vacuum Rabi splitting (blue solid curves) resulting from the coupling between the states $|e, 0\rangle$ and $|g, 3\rangle$ due to the presence of counterrotating terms in the system Hamiltonian. The energy splitting reaches its minimum at $\omega_q/2\pi \approx 11.89$ GHz $\approx 3(\omega_1^{\mathrm{r}}/2\pi)$. The anticrossing is not present in the JC model (red dashed curves), since it arises from the coherent coupling between states with a different number of excitations.

expressed as

$$\frac{1}{\sqrt{2}}(|e,0\rangle \pm |g,2\rangle).\tag{12}$$

The second avoided crossing at higher energy corresponds to the second rung of the two-photon Rabi ladder and the corresponding approximated hybridized states (at the minimum splitting) are

$$\frac{1}{\sqrt{2}}(|e,1\rangle \pm |g,3\rangle).\tag{13}$$

The third smallest splitting, occurring at $\omega_q \approx 3\omega_1^r$, corresponds to a three-photon vacuum Rabi splitting. Here a single qubit is resonantly coupled with a three-photon state, resulting, at the minimum splitting, in the approximated eigenstates

$$\frac{1}{\sqrt{2}}(|e,0\rangle \pm |g,3\rangle).\tag{14}$$

Figure 6 displays the system dynamics after the arrival of a π-like pulse exciting the qubit described by the Hamiltonian (11). Specifically, Fig. 6(a) shows the time evolution of $\langle \hat{X}^- \hat{X}^+ \rangle$ and $\langle \hat{C}^- \hat{C}^+ \rangle$. Calculations have been carried out in the absence of pure dephasing ($\gamma_\phi = 0$). Vacuum Rabi oscillations showing the reversible excitation exchange between the qubit and the resonator are clearly visible. We observe that the mean intracavity physical photon number at its first maximum is very close to 3. This is an initial hint that when the qubit is in the ground state the resonator mode is in a three-photon state. The period of a complete population oscillation is $2\pi/\Omega_{\text{eff}}^{(3\text{ph})}$, where $2\Omega_{\text{eff}}^{(3\text{ph})}$ is the minimum splitting in Fig. 5(c).

Figure 6(b) displays the time evolution of the zero-delay three-photon correlation function $G^{(3)}(t) = \langle \hat{X}^-(t)\hat{X}^-(t)\hat{X}^-(t)\hat{X}^+(t)\hat{X}^+(t)\hat{X}^+(t)\rangle$ together with the intracavity photon number $\langle \hat{X}^-\hat{X}^+\rangle$ for comparison. At early times the peak values of $G^{(3)}(t)$ are approximately two times higher than those of the mean photon number $\langle \hat{X}^-(t)\hat{X}^+(t)\rangle$. This is a specific feature of three-photon Fock states and indicates an almost-perfect three-photon correlation. We observe that $G^{(3)}(t)$ at early times reaches a peak value slightly beyond 6. This indicates that the system has a non-negligible probability to emit more than three photons. This is confirmed by the presence of a nonzero four-photon correlation function. Analyzing the different transitions contributing to $G^{(3)}(t)$, we can attribute this effect to additional low-frequency transition $|4\rangle \rightarrow |3\rangle$. These transitions between Rabi-split states occur when parity symmetry is broken [33] and in this case produce a four-photon cascade $|4\rangle \rightarrow |3\rangle \rightarrow |2\rangle \rightarrow |1\rangle \rightarrow |0\rangle$. This small contribution cannot be observed if its low frequency is outside the frequency-detection window. Analogously to the two-photon case (see Fig. 4), pure dephasing does not significantly affect the dynamics of multiphoton quantum Rabi oscillations (plot not shown).

C. Generation of entangled Greenberger-Horne-Zeilinger states

Standard vacuum Rabi oscillations have been exploited for the realization of atom-atom entanglement (see, e.g., Ref. [2]). Here we show that the multiphoton Rabi oscillations can be directly applied to the deterministic realization of more complex entangled states. As an initial application we discuss
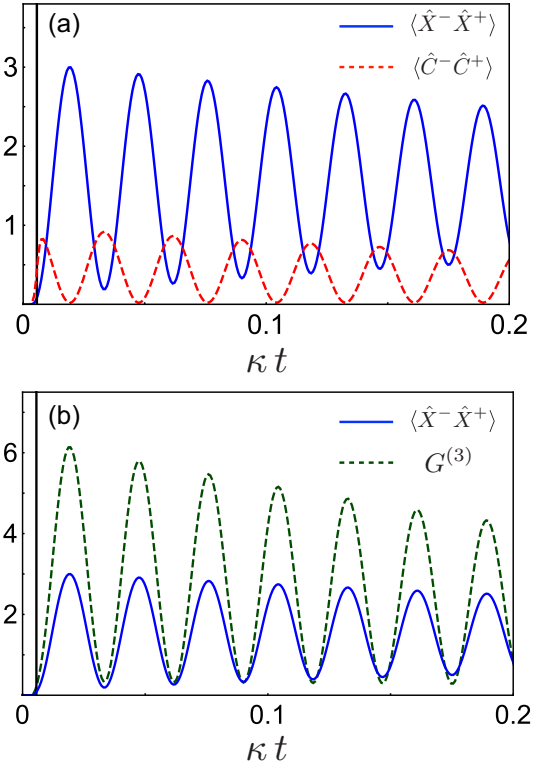

FIG. 6. (Color online) (a) Temporal evolution of the cavity mean photon number $\langle \hat{X}^- \hat{X}^+ \rangle$ (blue solid curve) and the qubit mean excitation number $\langle \hat{C}^- \hat{C}^+ \rangle$ (red dashed curve) after the arrival of a π-like Gaussian pulse exciting the qubit (the black vertical line on the far left shows the wave-packet center time). The amplitude and the central frequency of the pulse are $A/\omega_1^r = 9.4 \times 10^{-2}$ and $\omega = (\omega_{4,0} + \omega_{3,0})/2$, respectively. After the arrival of the pulse, the system undergoes vacuum Rabi oscillations showing the reversible excitation exchange between the qubit and the resonator. The fact that the mean intracavity physical photon number at its first maximum is very close to 3 is an initial signature that, when the qubit is in its ground state, the resonator mode is in a three-photon state. (b) Time evolution of the zero-delay three-photon function $G^{(3)}(t)$ (dashed green curve) together with the intracavity photon number $\langle \hat{X}^- \hat{X}^+ \rangle$ (solid blue curve). The first peak value of the three-photon correlation function is approximately two times higher than that of the mean photon number, a signature of an almost-perfect three-photon correlation. The parameters for the resonator and qubit losses are the same as in Fig. 3.

the deterministic realization of multiatom Greenberger-Horne-Zeilinger (GHZ) states [49] by using only one resonator. The GHZ states lead to striking violations of local realism and are an important resource for quantum information processing [50], quantum cryptography [51], and error correction protocols [52]. Superconducting circuits have been used to study GHZ states (see, e.g., Refs. [53,54]).

Consider a resonator coupled to qubit 1 in the USC regime where two-photon vacuum Rabi oscillations can occur. The resonator also interacts in the strong- (not ultrastrong-) coupling regime with two additional qubits (2 and 3). Although the coupling rates between the resonator and the qubits are fixed, the qubit-resonator interaction can be switched on and

off by adjusting the qubit frequencies [14]. The protocol is simple and consists of three steps, one for each qubit. The different qubits do not interact directly with each other. They interact one at a time with the same resonator. We start by exciting the ultrastrongly coupled qubit 1 with a π pulse. Then, by changing the flux offset (at time $t = 0$), we drive it into resonance with the two-photon state of the resonator [Fig. 1(c)]. The system state at time t is $|\psi\rangle = \cos{(\Omega_{\text{eff}}^{(2\text{ph})}t)}|e,g,g,0\rangle + \sin{(\Omega_{\text{eff}}^{(2\text{ph})}t)}|g,g,g,2\rangle$. We let the qubit interact for a $\pi/2$ Rabi rotation so that the resulting state is

$$\frac{1}{\sqrt{2}}(|e,g,g,0\rangle + |g,g,g,2\rangle). \tag{15}$$

We then drive the qubit back out of resonance, stopping the Rabi rotation. The new state of the system now consists of the Einstein-Podolsky-Rosen pair constituted by qubit 1 and the resonator described in Eq. (15). Detecting qubit 1 in a given quantum state instantaneously collapses the cavity mode in the correlated field state. For example, detecting this qubit in the ground state $|g\rangle$ amounts to preparing a *two-photon* Fock state in the cavity. Qubits 2 and 3 are still in a factorized state.

The second step consists of driving qubit 2 into resonance with the one-photon state of the first resonator mode for a π rotation time so that the resulting state is $(|e,g,g,0\rangle - |g,e,g,1\rangle)/\sqrt{2}$. For the third step, we similarly drive the third qubit into resonance with the first resonator mode for a π rotation. The resulting state is $(|e,g,g,0\rangle + |g,e,e,0\rangle)/\sqrt{2}$. At this point, the photon state can be factored out, leaving us with a three-qubit GHZ-like entangled state. We note that the excitation of qubits 2 and 3 is conditioned on the presence of photons in the resonator. The excitation swapping between the resonator and qubits 2 and 3 carries away the cavity photons and transfers the entanglement of qubit 1 with the resonator to the other two qubits. A more conventional GHZ state can be obtained by performing a final local operation on qubit 1, e.g., by sending a further π pulse to the first qubit, so that the resulting final state is $(|g,g,g,0\rangle + |e,e,e,0\rangle)/\sqrt{2}$. This procedure can be easily generalized to four or more qubits. In general, if n-photon Rabi oscillations are achieved, then $(n + 1)$-qubit GHZ states can be produced. We note that this protocol does not need the initial synthesis of photonic or atomic superposition states [55,56].

IV. CONCLUSION

We have investigated vacuum Rabi oscillations in the USC regime. According to the Jaynes-Cummings model, the qubit and the resonator can exchange a single excitation quantum through a coherent Rabi oscillation process. Such Rabi oscillations play a key role in the manipulation of atomic and field states for quantum information processing [12]. Our theoretical predictions show clear evidence for physics beyond the Jaynes-Cummings model and extend the concept of quantum Rabi oscillations. We find that multiphoton reversible exchanges between an individual qubit and a resonator can be observed in the USC regime. Specifically, we have shown that experimental state-of-the-art circuit-QED systems can undergo two- and three-photon vacuum Rabi oscillations. Still increasing the coupling rate, a higher number of photons can

be exchanged with the qubit during a single Rabi oscillation. These anomalous Rabi oscillations can be exploited for the realization of efficient Fock-state sources of light and for the implementation of novel protocols for the control and manipulation of atomic and field states.

APPENDIX: ANALYTICAL DERIVATION OF THE TWO-PHOTON-QUBIT EFFECTIVE HAMILTONIAN

In this Appendix we derive the analytical expression for the effective Hamiltonian in Eq. (9), describing the two-photon coupling between the states $|e,0\rangle$ and $|g,2\rangle$. We start from the reduced Hamiltonian in Eq. (8) and then move to the rotating frame with frequency $\omega_{\text{q}}/2$, obtaining the transformed reduced Hamiltonian

$$\frac{\hat{H}_{\text{r}}'}{\hbar} = \begin{pmatrix} 0 & g_1 \sin\theta & g_1 \cos\theta & 0 \\ g_1 \sin\theta & \omega_1^{\text{r}} & 0 & \sqrt{2}g_1 \cos\theta \\ g_1 \cos\theta & 0 & \omega_1^{\text{r}} - \omega_{\text{q}} & -\sqrt{2}g_1 \sin\theta \\ 0 & \sqrt{2}g_1 \cos\theta & -\sqrt{2}g_1 \sin\theta & 2\omega_1^{\text{r}} - \omega_{\text{q}}. \end{pmatrix}. \tag{A1}$$

Now the order of columns and rows is $|e,0\rangle$, $|e,1\rangle$, $|g,1\rangle$, and $|g,2\rangle$. After the transformation, an arbitrary state of the system in this truncated Hilbert space can be denoted by $(c1,c2,c3,c4)^T$ and the Schrödinger equation with Hamiltonian $\hat{H}_{\text{r}}'$ gives

$$i\dot{c}_1 = (g_1 \sin\theta)c_2 + (g_1 \cos\theta)c_3, \tag{A2}$$

$$i\dot{c}_2 = \omega_1^{\text{r}}c_2 + (g_1 \sin\theta)c_1 + (\sqrt{2}g_1 \cos\theta)c_4, \tag{A3}$$

$$i\dot{c}_3 = (\omega_1^{\text{r}} - \omega_{\text{q}})c_3 + (g_1 \cos\theta)c_1 - (\sqrt{2}g_1 \sin\theta)c_4, \tag{A4}$$

$$i\dot{c}_4 = (2\omega_1^{\text{r}} - \omega_{\text{q}})c_4 + (\sqrt{2}g_1 \cos\theta)c_2 - (\sqrt{2}g_1 \sin\theta)c_3. \tag{A5}$$

For $g_1/\omega_1^{\text{r}} \ll 1$, the adiabatic elimination in Eqs. (A3) and (A4) can be applied [39] and the coefficients c_2 and c_3 can be approximated as

$$c_2 \approx -\frac{g_1}{\omega_1^{\text{r}}}(\sin\theta c_1 + \sqrt{2}\cos\theta c_4), \tag{A6}$$

$$c_3 \approx -\frac{g_1}{(\omega_1^{\text{r}} - \omega_{\text{q}})}(\cos\theta c_1 - \sqrt{2}\sin\theta c_4). \tag{A7}$$

The coupled equations for c_1 and c_4 are obtained by substituting these results in Eqs. (A2) and (A5):

$$i\dot{c}_1 \approx \frac{g_1^2\left(\omega_{\mathrm{q}}\sin^2(2\theta) - \omega_1^{\mathrm{r}}\right)}{\omega_1^{\mathrm{r}}\left(\omega_1^{\mathrm{r}} - \omega_{\mathrm{q}}\right)}c_1 + \frac{\sqrt{2}g_1^2\omega_{\mathrm{q}}\sin(2\theta)}{2\omega_1^{\mathrm{r}}\left(\omega_1^{\mathrm{r}} - \omega_{\mathrm{q}}\right)}c_4, \quad \text{(A8)}$$

$$i\dot{c}_4 \approx \frac{-2g_1^2\left(\omega_1^{\mathrm{r}} - \omega_{\mathrm{q}}\cos^2\theta\right) + \omega_1^{\mathrm{r}}\left[2\left(\omega_1^{\mathrm{r}}\right)^2 - 3\omega_1^{\mathrm{r}}\omega_{\mathrm{q}} + \omega_{\mathrm{q}}^2\right]}{\omega_1^{\mathrm{r}}\left(\omega_1^{\mathrm{r}} - \omega_{\mathrm{q}}\right)}c_4$$
$$+ \frac{\sqrt{2}g_1^2\omega_{\mathrm{q}}\sin(2\theta)}{2\omega_1^{\mathrm{r}}\left(\omega_1^{\mathrm{r}} - \omega_{\mathrm{q}}\right)}c_1. \quad \text{(A9)}$$

Considering the near-resonance case $\omega_1^{\mathrm{r}} \approx \omega_{\mathrm{q}}/2$, transforming back to the laboratory frame and keeping only the g_1^2 dependence terms in the diagonal elements, the effective Hamiltonian in Eq. (9) is obtained. According to the effective Hamiltonian (9), the ratio of the minimum splitting at the avoided crossing [see Fig. 1(c)] to the qubit frequency ω_{q} is given by

$$\frac{2\Omega_{\mathrm{eff}}^{(2\mathrm{ph})}}{\omega_{\mathrm{q}}} = 4\sqrt{2}\sin(2\theta)\left(\frac{g_1}{\omega_{\mathrm{q}}}\right)^2. \quad \text{(A10)}$$
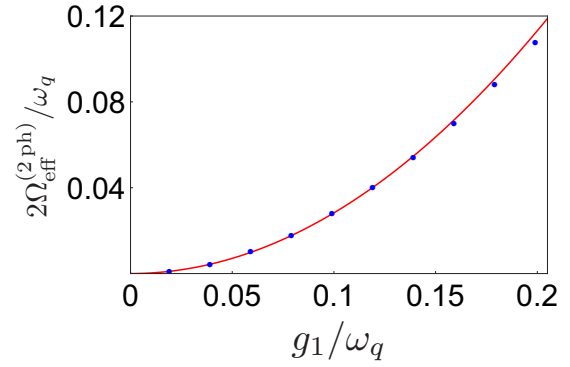

FIG. 7. (Color online) Comparison between the minimum energy splitting $2\Omega_{\mathrm{eff}}^{(2\mathrm{ph})}/\omega_{\mathrm{q}}$ obtained analytically (red solid curve) and numerically (blue points) as a function of g_1/ω_{q} for $\theta = \pi/4$.

A comparison between analytical and numerical results for the minimum energy splitting $2\Omega_{\mathrm{eff}}^{(2\mathrm{ph})}/\omega_{\mathrm{q}}$ is shown in Fig. 7 as a function of g_1/ω_{q}.

[1] M. Brune, F. Schmidt-Kaler, A. Maali, J. Dreyer, E. Hagley, J. M. Raimond, and S. Haroche, Quantum Rabi Oscillation: A Direct Test of Field Quantization in a Cavity, Phys. Rev. Lett. **76**, 1800 (1996).

[2] J. M. Raimond, M. Brune, and S. Haroche, Manipulating quantum entanglement with atoms and photons in a cavity, Rev. Mod. Phys. **73**, 565 (2001).

[3] R. J. Thompson, G. Rempe, and H. J. Kimble, Observation of Normal-Mode Splitting for an Atom in an Optical Cavity, Phys. Rev. Lett. **68**, 1132 (1992).

[4] S. Haroche and J. M. Raimond, *Exploring the Quantum: Atoms, Cavities and Photons* (Oxford University Press, Oxford, 2006).

[5] A. Auffeves, D. Gerace, R. Maxime, S. Portolan, M. F. Santos, L. C. Kwek, and C. Miniatura, *Strong Light-Matter Coupling: From Atoms to Solid-State Physics* (World Scientific, Singapore, 2013).

[6] T. Yoshie, A. Scherer, J. Hendrickson, G. Khitrova, H. M. Gibbs, G. Rupper, C. Ell, O. B. Shchekin, and D. G. Deppe, Vacuum Rabi splitting with a single quantum dot in a photonic crystal nanocavity, Nature (London) **432**, 200 (2004).

[7] J. P. Reithmaier, G. Sek, A. Löffler, C. Hofmann, S. Kuhn, S. Reitzenstein, L. V. Keldysh, V. D. Kulakovskii, T. L. Reinecke, and A. Forchel, Strong coupling in a single quantum dot–semiconductor microcavity system, Nature (London) **432**, 197 (2004).

[8] A. Blais, R. S. Huang, A. Wallraff, S. M. Girvin, and R. J. Schoelkopf, Cavity quantum electrodynamics for superconducting electrical circuits: An architecture for quantum computation, Phys. Rev. A **69**, 062320 (2004).

[9] A. Wallraff, D. I. Schuster, A. Blais, L. Frunzio, R. S. Huang, J. Majer, S. Kumar, S. M. Girvin, and R. J. Schoelkopf, Strong coupling of a single photon to a superconducting qubit using circuit quantum electrodynamics, Nature (London) **431**, 162 (2004).

[10] I. Chiorescu, P. Bertet, K. Semba, Y. Nakamura, C. J. P. M. Harmans, and J. E. Mooij, Coherent dynamics of a flux qubit coupled to a harmonic oscillator, Nature (London) **431**, 159 (2004).

[11] J. Q. You and F. Nori, Atomic physics and quantum optics using superconducting circuits, Nature (London) **474**, 589 (2011).

[12] S. Haroche, Nobel lecture: Controlling photons in a box and exploring the quantum to classical boundary, Rev. Mod. Phys. **85**, 1083 (2013).

[13] S. Deleglise, I. Dotsenko, C. Sayrin, J. Bernu, M. Brune, J. M. Raimond, and S. Haroche, Reconstruction of non-classical cavity field states with snapshots of their decoherence, Nature (London) **455**, 510 (2008).

[14] M. Hofheinz, H. Wang, M. Ansmann, R. C. Bialczak, E. Lucero, M. Neeley, A. D. O'Connell, D. Sank, J. Wenner, J. M. Martinis, and A. N. Cleland, Synthesizing arbitrary quantum states in a superconducting resonator, Nature (London) **459**, 546 (2009).

[15] S. Haroche, M. Brune, and J. M. Raimond, Atomic clocks for controlling light fields, Phys. Today **66**(1), 27 (2013).

[16] B. Vlastakis, G. Kirchmair, Z. Leghtas, S. E. Nigg, L. Frunzio, S. M. Girvin, M. Mirrahimi, M. H. Devoret, and R. J. Schoelkopf, Deterministically encoding quantum information using 100-photon Schrödinger cat states, Science **342**, 607 (2013).

[17] J. Q. You and F. Nori, Superconducting circuits and quantum information, Phys. Today **58**(11), 42 (2005).

[18] H. J. Kimble, The quantum internet, Nature (London) **453**, 1023 (2008).

[19] G. Günter, A. A. Anappara, J. Hees, A. Sell, G. Biasiol, L. Sorba, S. De Liberato, C. Ciuti, A. Tredicucci, A. Leitenstorfer, and R. Huber, Sub-cycle switch-on of ultrastrong light–matter interaction, Nature (London) **458**, 178 (2009).

[20] P. Forn-Díaz, J. Lisenfeld, D. Marcos, J. J. García-Ripoll, E. Solano, C. J. P. M. Harmans, and J. E. Mooij, Observation of the Bloch-Siegert Shift in a Qubit-Oscillator System in the

Ultrastrong Coupling Regime, Phys. Rev. Lett. **105**, 237001 (2010).

[21] T. Niemczyk, F. Deppe, H. Huebl, E. P. Menzel, F. Hocke, M. J. Schwarz, J. J. García-Ripoll, D. Zueco, T. Hümmer, E. Solano, A. Marx, and R. Gross, Circuit quantum electrodynamics in the ultrastrong-coupling regime, Nat. Phys. **6**, 772 (2010).

[22] T. Schwartz, J. A. Hutchison, C. Genet, and T. W. Ebbesen, Reversible Switching of Ultrastrong Light-Molecule Coupling, Phys. Rev. Lett. **106**, 196405 (2011).

[23] M. Geiser, F. Castellano, G. Scalari, M. Beck, L. Nevou, and J. Faist, Ultrastrong Coupling Regime and Plasmon Polaritons in Parabolic Semiconductor Quantum Wells, Phys. Rev. Lett. **108**, 106402 (2012).

[24] G. Scalari, C. Maissen, D. Turčinková, D. Hagenmüller, S. De Liberato, C. Ciuti, C. Reichl, D. Schuh, W. Wegscheider, M. Beck, and J. Faist, Ultrastrong coupling of the cyclotron transition of a 2D electron gas to a THz metamaterial, Science **335**, 1323 (2012).

[25] S. Gambino, M. Mazzeo, A. Genco, O. Di Stefano, S. Savasta, S. Patane, D. Ballarini, F. Mangione, G. Lerario, D. Sanvitto, and G. Gigli, Exploring light–matter interaction phenomena under ultrastrong coupling regime, ACS Photon. **1**, 1042 (2014).

[26] M. Goryachev, W. G. Farr, D. L. Creedon, Y. Fan, M. Kostylev, and M. E. Tobar, High-Cooperativity Cavity QED with Magnons at Microwave Frequencies, Phys. Rev. Appl. **2**, 054002 (2014).

[27] C. Maissen, G. Scalari, F. Valmorra, M. Beck, J. Faist, S. Cibella, R. Leoni, C. Reichl, C. Charpentier, and W. Wegscheider, Ultrastrong coupling in the near field of complementary split-ring resonators, Phys. Rev. B **90**, 205309 (2014).

[28] S. De Liberato, C. Ciuti, and I. Carusotto, Quantum Vacuum Radiation Spectra from a Semiconductor Microcavity with a Time-Modulated Vacuum Rabi Frequency, Phys. Rev. Lett. **98**, 103602 (2007).

[29] S. Ashhab and F. Nori, Qubit-oscillator systems in the ultrastrong-coupling regime and their potential for preparing nonclassical states, Phys. Rev. A **81**, 042311 (2010).

[30] X. Cao, J. Q. You, H. Zheng, A. G. Kofman, and F. Nori, Dynamics and quantum Zeno effect for a qubit in either a low-or high-frequency bath beyond the rotating-wave approximation, Phys. Rev. A **82**, 022119 (2010).

[31] X. Cao, J. Q. You, H. Zheng, and F. Nori, A qubit strongly coupled to a resonant cavity: Asymmetry of the spontaneous emission spectrum beyond the rotating wave approximation, New J. Phys. **13**, 073002 (2011).

[32] A. Ridolfo, M. Leib, S. Savasta, and M. J. Hartmann, Photon Blockade in the Ultrastrong Coupling Regime, Phys. Rev. Lett. **109**, 193602 (2012).

[33] A. Ridolfo, S. Savasta, and M. J. Hartmann, Nonclassical Radiation from Thermal Cavities in the Ultrastrong Coupling Regime, Phys. Rev. Lett. **110**, 163601 (2013).

[34] R. Stassi, A. Ridolfo, O. Di Stefano, M. J. Hartmann, and S. Savasta, Spontaneous Conversion from Virtual to Real Photons in the Ultrastrong-Coupling Regime, Phys. Rev. Lett. **110**, 243601 (2013).

[35] J.-F. Huang and C. K. Law, Photon emission via vacuum-dressed intermediate states under ultrastrong coupling, Phys. Rev. A **89**, 033827 (2014).

[36] A. Cacciola, O. Di Stefano, R. Stassi, R. Saija, and S. Savasta, Ultrastrong coupling of plasmons and excitons in a nanoshell, ACS Nano **8**, 11483 (2014).

[37] L. Garziano, R. Stassi, A. Ridolfo, O. Di Stefano, and S. Savasta, Vacuum-induced symmetry breaking in a superconducting quantum circuit, Phys. Rev. A **90**, 043817 (2014).

[38] A. Baust *et al.*, Ultrastrong coupling in two-resonator circuit QED, arXiv:1412.7372.

[39] K. K. W. Ma and C. K. Law, Three-photon resonance and adiabatic passage in the large-detuning Rabi model, Phys. Rev. A **92**, 023842 (2015).

[40] S. De Liberato, D. Gerace, I. Carusotto, and C. Ciuti, Extracavity quantum vacuum radiation from a single qubit, Phys. Rev. A **80**, 053810 (2009).

[41] F. Beaudoin, J. M. Gambetta, and A. Blais, Dissipation and ultrastrong coupling in circuit QED, Phys. Rev. A **84**, 043832 (2011).

[42] L. Garziano, A. Ridolfo, R. Stassi, O. Di Stefano, and S. Savasta, Switching on and off of ultrastrong light-matter interaction: Photon statistics of quantum vacuum radiation, Phys. Rev. A **88**, 063829 (2013).

[43] S. Agarwal, S. M. Hashemi Rafsanjani, and J. H. Eberly, Dissipation of the Rabi model beyond the Jaynes-Cummings approximation: quasi-degenerate qubit and ultra-strong coupling, J. Phys. B **46**, 224017 (2013).

[44] H.-P. Breuer and F. Petruccione, *The Theory of Open Quantum Systems* (Oxford University Press, Oxford, 2002).

[45] E. T. Jaynes and F. W. Cummings, Comparison of quantum and semiclassical radiation theories with application to the beam maser, Proc. IEEE **51**, 89 (1963).

[46] Y. X. Liu, J. Q. You, L. F. Wei, C. P. Sun, and F. Nori, Optical Selection Rules and Phase-Dependent Adiabatic State Control in a Superconducting Quantum Circuit, Phys. Rev. Lett. **95**, 087001 (2005).

[47] D. Braak, Integrability of the Rabi model, Phys. Rev. Lett. **107**, 100401 (2011).

[48] J. Johansson, S. Saito, T. Meno, H. Nakano, M. Ueda, K. Semba, and H. Takayanagi, Vacuum Rabi Oscillations in a Macroscopic Superconducting Qubit LC Oscillator System, Phys. Rev. Lett. **96**, 127006 (2006).

[49] D. M. Greenberger, M. A. Horne, A. Shimony, and A. Zeilinger, Bell's theorem without inequalities, Am. J. Phys. **58**, 1131 (1990).

[50] S. Bose, V. Vedral, and P. L. Knight, Multiparticle generalization of entanglement swapping, Phys. Rev. A **57**, 822 (1998).

[51] R. Cleve, D. Gottesman, and H.-K. Lo, How to Share a Quantum Secret, Phys. Rev. Lett. **83**, 648 (1999).

[52] D. P. Di Vincenzo and P. W. Shor, Fault-Tolerant Error Correction with Efficient Quantum Codes, Phys. Rev. Lett. **77**, 3260 (1996).

[53] L. F. Wei, Y. X. Liu, and F. Nori, Generation and Control of Greenberger-Horne-Zeilinger Entanglement in Superconducting Circuits, Phys. Rev. Lett. **96**, 246803 (2006).

[54] C.-P. Yang, Q.-P. Su, S.-B. Zheng, and F. Nori, Entangling superconducting qubits in a multi-cavity system, arXiv:1506.06108.

[55] J. I. Cirac and P. Zoller, Preparation of macroscopic superpositions in many-atom systems, Phys. Rev. A **50**, R2799 (1994).

[56] S.-B. Zheng, One-Step Synthesis of Multiatom Greenberger-Horne-Zeilinger States, Phys. Rev. Lett. **87**, 230404 (2001).